

Multi-point measurements of the plasma properties inside an aurora from the SPIDER sounding rocket.

G. Giono^{1,2}, N. Ivchenko¹, T. Sergienko³ and U. Brändström³

¹Department of Space and Plasma Physics, KTH-Royal Institute of Technology, Stockholm, Sweden

²Leibniz Institute of Atmospheric Physics at the Rostock University (IAP), Kühlungsborn, Germany

³IRF-Swedish Institute of Space Physics, Kiruna, Sweden

Key Points:

- Multi-point *in situ* measurement of plasma properties.
- Auroral study.
- Sounding rocket instrumentation.
- Sheath simulation.

Corresponding author: G. Giono, ggiono@kth.se

Abstract

The Small Payloads for Investigation of Disturbances in Electrojet by Rockets (SPIDER) sounding rocket was launched on February 2nd 2016 (21:09 UT), deploying ten free falling units (FFUs) inside a westward travelling auroral surge. Each FFUs deployed spherical electric field and Langmuir probes on wire-booms, providing *in situ* multi-point recordings of the electric field and plasma properties.

The analytical retrieval of the plasma parameters, namely the electron density, electron temperature and plasma potential, from the Langmuir probe measurements was non-trivial due to sheath effects and detailed explanation are discussed in this article. An empirical assumption on the sheath thickness was required, which was confirmed by simulating the plasma environment around the FFU using the Spacecraft Plasma Interaction Software (SPIS). In addition, the retrieved electron density and temperature are also in agreement with the simultaneous incoherent scatter radar measurements from the EISCAT facility. These two independent confirmations provided a good level of confidence in the plasma parameters obtained from the FFUs, and events observed during the flight are discussed in more details. Hints of drift-wave instabilities and Hall current introduced by increased electron precipitation inside a region of enhanced density were observed by the FFUs.

1 Introduction

Auroral electrojet are atmospheric optical emission seen at polar latitude. These phenomena are created by the precipitation of energetic particles from outer space (*e.g.* solar wind) being funnelled along Earth's magnetic field lines and ionizing the atomic elements present in the atmosphere by collision. Auroras typically occur in the E region, the lowest part of the ionosphere located at heights between 100 and 120 kilometers. This region holds still some important scientific questions, as the dynamic of the micro processes is not fully understood.

The Small Payloads for Investigation of Disturbances in Electrojet by Rockets (SPIDER) sounding rocket experiment was designed to investigate the various spatial and temporal scales of these phenomena, in particular the Farley-Buneman instability which induces a relative drift motion between ions and electrons and is expected to occur at altitudes between 85 and 95 km. Such instability possibly leads to electrostatic waves, predicted by theory and MHD simulations [Oppenheim and Dimant, 2013] but not yet observed experimentally. Multi-point measurements are achieved by ejecting ten identical disc-shape free falling units (FFUs) from the rocket, each equipped with a suite of instruments to characterize the plasma and electromagnetic properties of the aurora: four spherical electric field probes deployed on 2 m booms recording the 2-dimensional projection of the electric field in the spin-plane of the FFU, four spherical Langmuir probes on 1 m booms for the plasma properties (*i.e.* density and temperature, plasma potential) and a fluxgate sensor for the magnetic field. The SPIDER rocket was launched on February 2nd 2016 (21:09 UT) from the Esrange space center in northern Sweden.

In this article, a detailed analysis of the Langmuir probe measurements from two out of the six recovered FFU is presented. The instrument and measurements are first introduced in Section 2. An overview of the analytical methodology used to retrieve the plasma parameters is given in Section 3, with further details discussed in Appendix A. These results were compared to a hybrid plasma simulation of the FFU and its Langmuir probe using the Spacecraft Plasma Interaction Software (SPIS), shown in Appendix B. The retrieved parameters are also compared to the simultaneous incoherent scatter radar measurements from EISCAT taken along the rocket path in Section 4. With confidence in the FFU measurements, Section 5 discussed two particularly interesting events seen during the flight. Finally, Section 6 summarizes the difficulties of interpreting Langmuir probe measurements in intermediate sheath regime and discusses possible improvement for future flights.

2 Langmuir probe measurements

Langmuir probes can be used to estimate plasma properties such as its density and temperature by recording the current-voltage characteristic of the plasma, *i.e.* the I - V curve. This is achieved by fixing the probe potential (*i.e.* probe bias) with respect to the FFU hull and recording the current induced as the plasma responds to the probe potential. The I - V curve is recorded by performing measurements at various probe biases, which is also referred as sweeps.

Each SPIDER FFU carried four gold-coated spherical Langmuir probes ($r = 12.5$ mm) deployed on 1 meter long wire-boom. Two out of the four probes operated short sweeps between -0.5 V to $+0.5$ V, whereas a third probe was operating long sweeps from -3 V to $+1.5$ V. The remaining probe was set to a fixed voltage bias of -5 V, monitoring fluctuation of the ion current. The recording electronic was designed with an adjustable gain amplifier automatically scaling the current range: the finest resolution range was between -150 pA and $+250$ pA whereas the largest range available was between -150 nA and $+250$ nA.

However, the plasma condition encountered during the flight led to a larger than expected current being collected. In addition, an unexpectedly large payload charging of -0.8 V was observed. This shifted the sweeps towards the ion branch, saturating all measurements from the short sweep and fixed bias Langmuir probes. As a result, only a limited part of the long-sweep had unsaturated measurements of the current. Short-circuits between the wire-booms and the hull induced by the wobble motion of the FFU also compromised the measurements from some FFUs. Figure 1 shows the usable measurements from FFU02 and FFU06, for bias between -0.1 V to -0.7 V, respectively sampling from the ion saturation current to the foot of the exponentially increasing electron current. Some short-circuits can be seen in FFU02 between 145 and 155 s, as well as around 210 s.

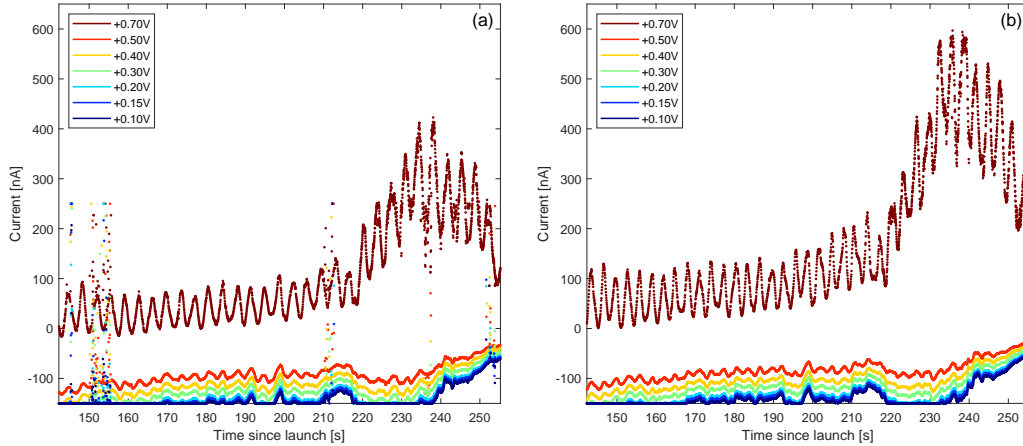


Figure 1. Langmuir probe measurements for FFU02 (a) and FFU06 (b) from 145 s to 255 s after launch. Colors dots show the current measured by the probe for the various voltage biases with respect to the hull. The large variability of the measured current seen for FFU02 around 150 s is due to the wobble-induced short-circuits between the boom and the hull.

3 Analytical retrieval of the plasma parameters

Given the proper analytic formulation of the ion saturation current and electron exponential electron current, one can retrieve the plasma parameters from the Langmuir probe current-voltage characteristic. Although the theory of current collection by a Langmuir probe is a well studied topic, both in the laboratory and onboard spacecrafts [Mott-Smith and Langmuir, 1926; Sagalyn *et al.*, 1963; Fahleson *et al.*, 1974; Pedersen *et al.*, 2008], its analytical treatment can quickly become

complicated due to sheath effects. The sheath is the region around the probe where the plasma quasi-neutrality breaks down due to the intrusive electric potential induced by the probe, and can affect the ion collection. For simplicity of treatment, most of the analytical formulations are generally derived in one of the two following regimes: thin-sheath or large-sheath (also known as orbital motion limit regime), where the sheath thickness is either negligible or much larger than the probe radius, respectively. Following this reasoning, Langmuir probes are usually designed to operate in one of these two regimes based on the expected plasma density and temperature to be probed. However, the presented case does not fall into either of these two extreme regimes, but rather in an intermediate regime where the sheath thickness is comparable to the probe radius. In addition, collection of ions by the probe motion through the plasma also needs to be accounted for, as the FFUs were moving at a velocity ranging from 200 m/s at apogee (*i.e.* lateral velocity) to more than 1000 m/s in the up and down-legs.

The collected current I is formulated as the sum of both the electron current I_{electron} minus the ion current I_{ion} as

$$I = I_{\text{electron}} + I_{\text{ion}} \quad (1)$$

The electron current in the transition region is expressed as an exponential function of the electron temperature T_e

$$I_{\text{electron}} = 4\pi r^2 n e \sqrt{\frac{k_B T_e}{2\pi m_e}} e^{e(V - V_p)/(k_B T_e)} \quad (2)$$

where r is the radius of the spherical probe, k_B is the Boltzmann constant and m_e is the mass of the electron. The factor in front of the exponential corresponds to the current collected by the thermal motion of the electron, assuming a Maxwellian distribution.

Similarly, the ion saturation current is expressed as

$$I_{\text{ion}} = -4\pi r^2 n e \sqrt{\frac{k_B T_i}{2\pi m_i}} I_{\text{acc}} \quad (3)$$

where the current collected by the random motion of the ions is multiplied by a factor which includes the effect of the probe potential (*i.e.* attracting more ions as the potential becomes more negative) and the collection of ions as the probe moves through the plasma. This factor is denoted as I_{acc} , as it corresponds to the current induced by the ions accelerated towards the probe. In order to avoid shifting the focus on the analysis rather than on the results, the expression used for I_{acc} and the details about the rest of the analytical retrieval are presented in Appendix A. In short, an empirical estimation of the sheath thickness around the probe was required due to the Langmuir probe operating in an intermediate sheath regime (*i.e.* not thin nor large sheath regimes). With this assumption, Equation (1) was fitted on the measured current-voltage characteristics to obtain the plasma parameters (electron density, electron temperature and plasma potential). In addition, hybrid plasma simulations using the Spacecraft Plasma Interaction Software [SPIS, Roussel *et al.*, 2008] were used to reproduce the sheath thickness and the current-voltage characteristic of the probe, providing further confidence in the analytical retrieval. These simulations are presented in Appendix B.

Figure 2 shows the time-series of the electron density, electron temperature and plasma potential (with respect to the floating potential) along the flight of the two FFUs considered. For better display purposes, the obviously unrealistic values due to short-circuits were removed and the time-series were smoothed with a 0.2 s moving average filter. One can see the very good correlation between the parameters retrieved for the two different FFUs. Some periodicity between 3 and 4 s can be seen in the electron density, especially between 150 and 190 s. Such periods are similar to the FFU spin rate (~ 3.4 s) and could be due to the ambient electric field affecting the probe biases: although the probe bias was corrected for this effect using the electric field probe measurements, some residual might remain thus propagating to the retrieved plasma parameters.

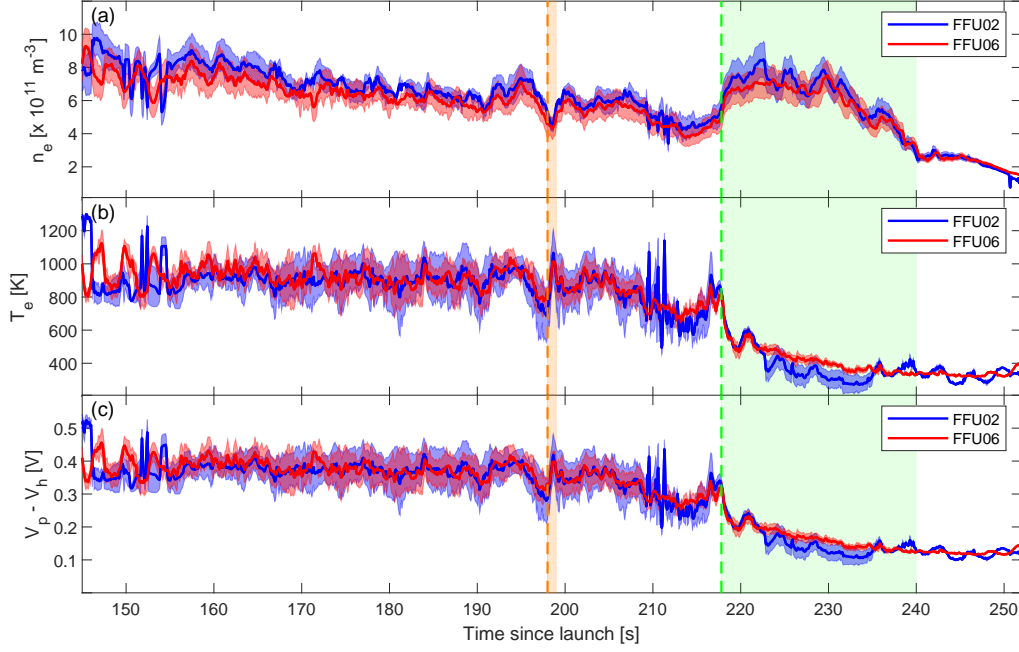


Figure 2. Time-series of the retrieved plasma parameters: electron density (a), electron temperature (b) and plasma potential with respect to hull potential (c). Solid lines show the average of the parameters obtained from the two fittings taken with different sheath thickness assumption ($s=1.0$ and $s=1.5$, see Appendix A). Shaded areas show the uncertainty taken as the difference between the mean and the results of the two fittings ($s=1.0$ and $s=1.5$). The vertical orange and green dash lines at 198 s and 218 s followed by the respective shaded columns refer to two events further discussed in Section 5.

4 Comparison with EISCAT incoherent scatter radar measurements

The EISCAT UHF facility in Tromsø, Norway, provided incoherent scatter radar measurements along the up-leg path of the rocket. The electron density and temperature were obtained from these measurements and compared to the plasma parameters obtained by the FFUs. Figure 3 displays the EISCAT measurements around the rocket's apogee along side the electron density and temperature for each FFU from Figure 2. Both measurements depicts a similar structure of the aurora, with a hot electron temperature around 1000 K above 110 km, with density around $5 \times 10^{11} \text{ m}^{-3}$, and a drop of both the density and the temperature (down to 400 K) in the down-leg part of the trajectory, below 110 km. This boundary between these two regions probably being the horizontal edge of the aurora. The remote measurements from EISCAT are another independent confirmation validating the plasma parameters measured by the FFUs.

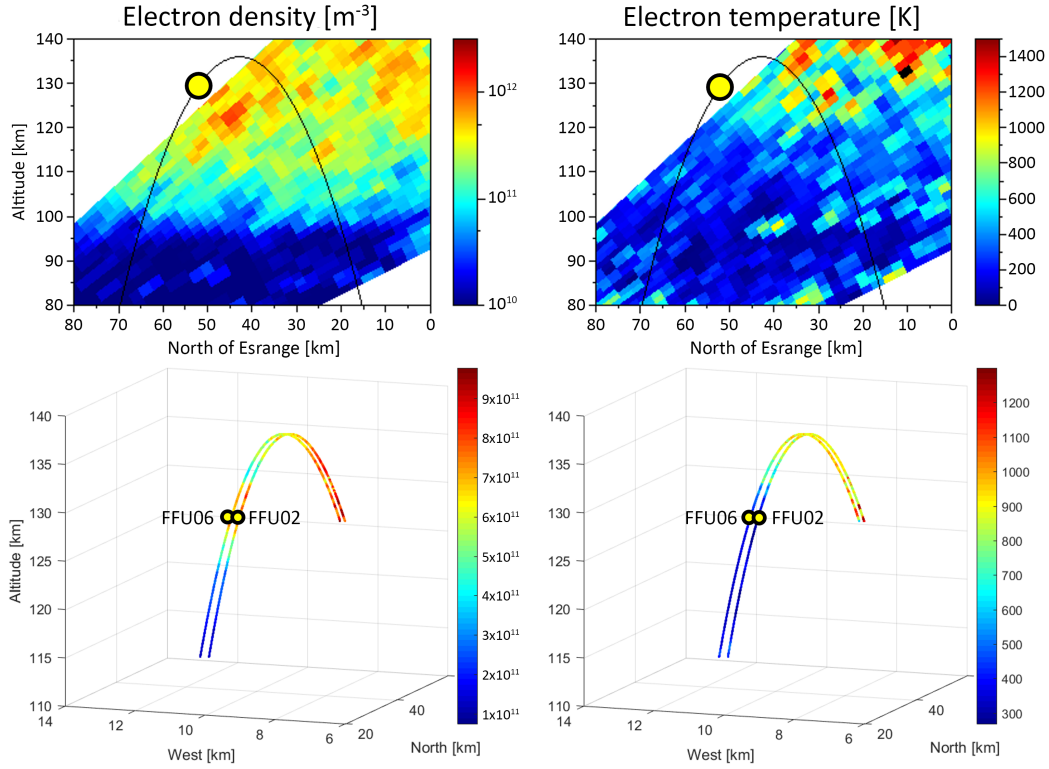


Figure 3. Snapshot of the electron density (left panels) and electron temperature (right panels) recorded by EISCAT along the up-leg part of the trajectory (top panels) and by the FFUs along the down-leg part of the trajectory (bottom panels). The yellow dots show the position of the FFUs at the time of the EISCAT measurement.

5 Hall current and turbulence inside a local plasma density enhancement

With confidence in the FFU measurements, a more detailed interpretation of the time-series shown in Figure 2 can be conducted. Two particular events can be seen in the time-series: a sharp decrease of the density and temperature with a rapid recovery around 198 s, and a significant increase in the density accompanied with a decrease in the electron temperature after 218 s and until ~ 240 s. These two events could either be spatial structures (*e.g.* auroral curtain), which of the FFUs were crossing, or temporal variation of the aurora (*e.g.* local precipitation along a field line). The second option is most likely for the first event, as the spatial scales on which the temperature drastically changes is less than a kilometer. This interpretation is also supported by the fact that no time-delay is seen between both FFUs, which were separated spatially by about 500 m in the horizontal plane. Interestingly, the change in the electron temperature seems to lead the change in density, as it can be seen to start increasing around 198 s while the electron density increased only ~ 0.5 s later. On the other hand the second event seems to be a local plasma density enhancement on larger spatial scale, *e.g.* a vertical auroral curtain crossed by the two FFUs along their down-leg parabolic trajectory, or a horizontal layer of enhanced ionisation (*i.e.* energy deposition region) in which the FFUs entered-in during the down-leg part of the trajectory. It is important to point out that, although the temporal resolution of the retrieved electron density and temperature was 0.05 s, no timing difference could be detected between the two FFUs. This indicates that these events were either faster (likely for the event at 198 s) or homogeneous on horizontal spatial scales between 100 and 1000 m, the horizontal separation between the FFUs (likely for the event between 218 and 240 s).

A closer look at context ground-based images from the Auroral Large Imaging System (ALIS, [Brändström, 2003]) provided additional hints to help interpreting this event. ALIS consists of four

imaging CCD cameras located around Kiruna. The systems provided multi-angle observations of the aurora green-line emission with a 10 s temporal resolution. Due to bad weather condition, only two out of the four stations could perform clear observation of the surge at the time of the flight. Nonetheless, a tomography-like reconstruction of the volume emission rate was carried out, and an overview around 200–260 s after lift-off is shown in Figure 4. One can see the volume emission rate increasing by a factor of two between 220 and 240 s, right where the electron density is also seen to double by the FFUs. The nature of this increase was further investigating by looking at the spatial and temporal variation of the volume emission rate, shown in Figure 5. The right column in Figure 5 clearly shows the FFUs entering a horizontal layer around 220 s where the volume emission rate increases by about two folds. The FFUs then exited this horizontal layer around 250 s. The westward motion of the aurora can be guessed in the left column of Figure 5 but does not seems to be the major contributor to the emission rate increase, thus ruling-out the vertical curtain possibility. The layer between 110 and 130 km have an emission rate ~ 1.5 times larger than the layers above and below these heights. In addition, the emission rate of this layer appears to increase by about 10 to 30% between 210 and 240 s compared before and after. The overall intensity of the auroral activity also greatly dropped after 250 s. Hence, the higher electron density seen by the FFUs around 220 s is likely due to an horizontal layer of enhanced ionisation as well as to a temporal increase in electron precipitation.

Note that ALIS did not provide enough temporal resolution to resolve the first event short duration (~ 1 s). However, the presence of an horizontal layer can be ruled out in this case, as such layers are unlikely of occur on such small scale height.

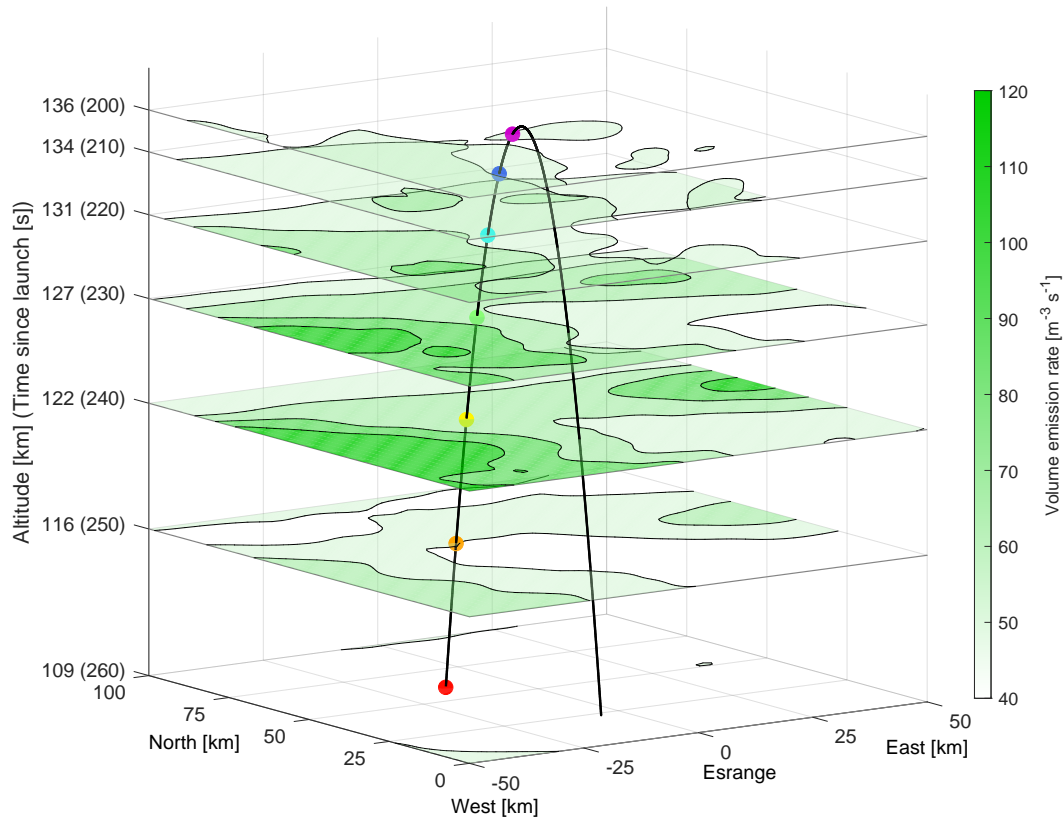


Figure 4. Tomography-like reconstruction of the aurora from ALIS observations. Each layer shows the volume emission rate for the various altitude, each taken at the time indicated on the z-axis. The black line shows the rocket trajectory, with the colored dots indicating the locations of the FFUs at each time.

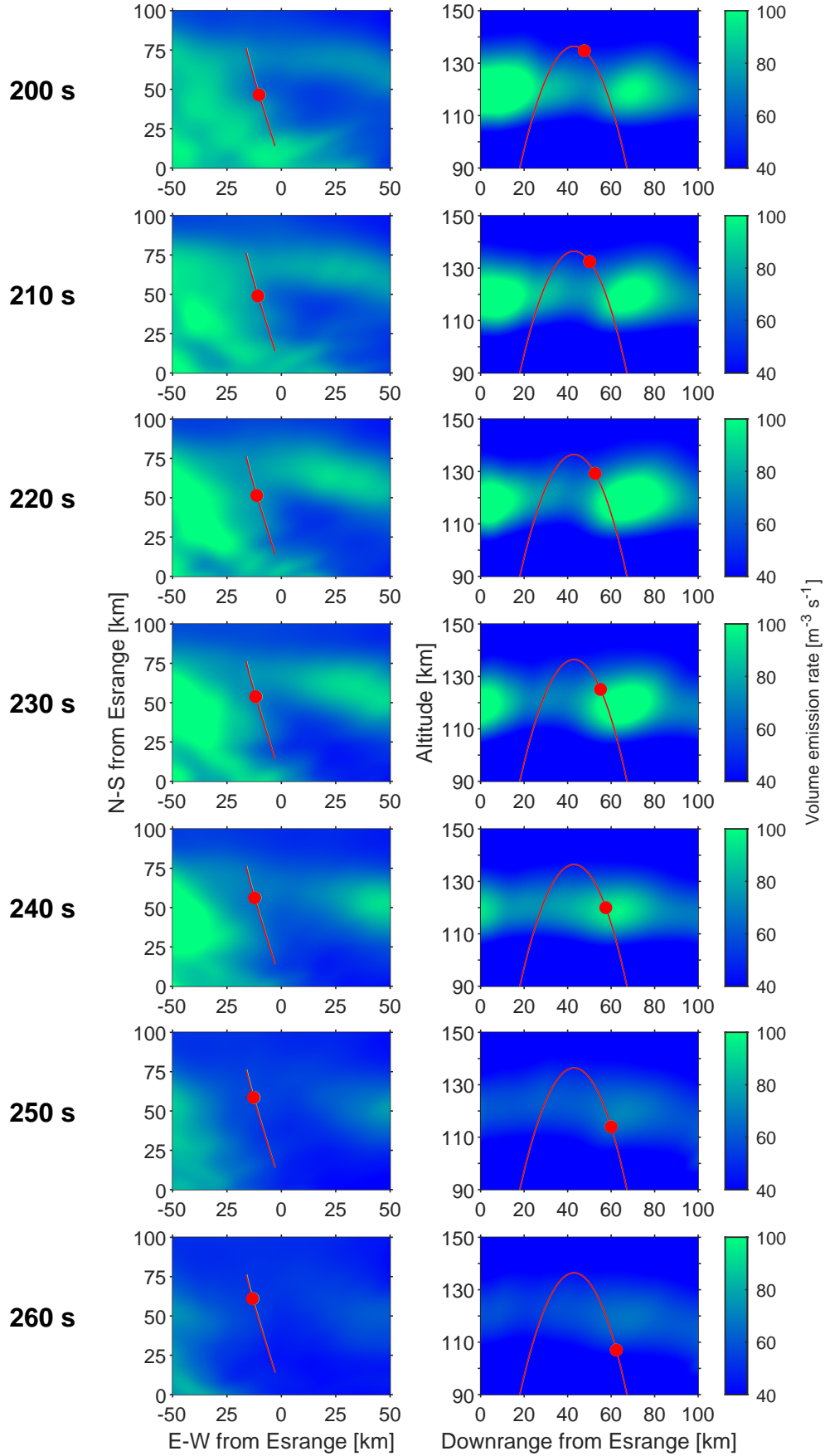


Figure 5. Timeline of the tomography-like reconstruction of the aurora from ALIS observations. The left column shows the top view integrated from 105 and 140 km altitude. The right column shows the vertical plane along the rocket trajectory. The red dots show the positions of the FFUs at each time along the trajectory, represented by the red line. The origin is centered on Esrang.

The horizontal layer with enhanced plasma density was investigated further by comparing the retrieved plasma parameters to the magnetic field measured by the SMILE fluxgate magnetometer, also onboard each FFU. Figure 6(a) and (c) shows the electron density and temperature while (d) shows the residual of the total magnetic field measured by the magnetometer after removing the expected field from the International Geomagnetic Reference Field (IGRF) model [Macmillan *et al.*, 2003] along the FFU trajectory. The total magnetic field in the density enhanced layer appears to be about 15 nT lower than expected from the model. This is an indication of Hall current in the region: a reduction of the magnetic field (along mostly the upward direction) is the results of an increased counter-clockwise $\mathbf{E} \times \mathbf{B}$ drift of the electron due to an increased electron current, *e.g.* from electron precipitation. Interestingly, the magnetic field perturbation does not set right when the FFUs encounter the over-dense region but lag slightly behind, about ~ 4 s (*i.e.* ~ 3 – 4 km vertically inside the layer). The magnetic field perturbation also seems to recover later (*i.e.* at lower heights) than the density: around 250 s compared to 240 s, which corresponds to roughly 10 km.

In addition, the plasma irregularities of the density enhancement region can also be studied using the electron density measurement. This is achieved by performing a Fast Fourier Transform of the detrended relative density on a 2 s moving window, following the method described by Spicher *et al.* [2014]. First the electron density in the 2 s window is detrended by removing a fitted linear relationship, effectively removing the very low frequencies. The detrended electron density is then normalized by its standard deviation and a Hanning window is applied to reduce edge irregularities effect before performing the Fast Fourier Transform. The slope of the resulting power spectrum contains information about how the energy dissipates locally, and Kintner and Seyler [1985] showed that this can be related to plasma instabilities, as different instabilities lead to different dissipation rates. Note that in the case of SPIDER's Langmuir probes, the slope was estimated from 1 Hz up to the Nyquist frequency of 10 Hz only, as the sampling rate of the I - V curves was limited to 20 Hz. Thus, the veracity of the results should be considered with caution. Nevertheless, the slope of detrended relative density power spectrum for both FFUs is shown in Figure 6(b). A slope of $-5/3$ can be seen in the stable region before 218 s, which is the signature of the typical Kolmogorov turbulent regime. However, the slope decreases to $-11/3$ in the region with enhanced density after 218 s. According to Kintner and Seyler [1985], this could be interpreted as a sign of a drift wave instability. In conclusion, the event starting at 218 s can be interpreted as a crossing of the FFUs into a horizontal layer of enhanced density at the same time as a temporal increase in electron precipitation. The higher precipitation in this layer induced Hall current, reducing the ambient magnetic field while also introducing a different turbulence regime by possibly fueling drift-wave instabilities. This is further supported by the fact that both the magnetic field perturbation and the measure of the turbulence regime seem to be correlated, both recovering around 250 s compared to 240 s for the density enhancement.

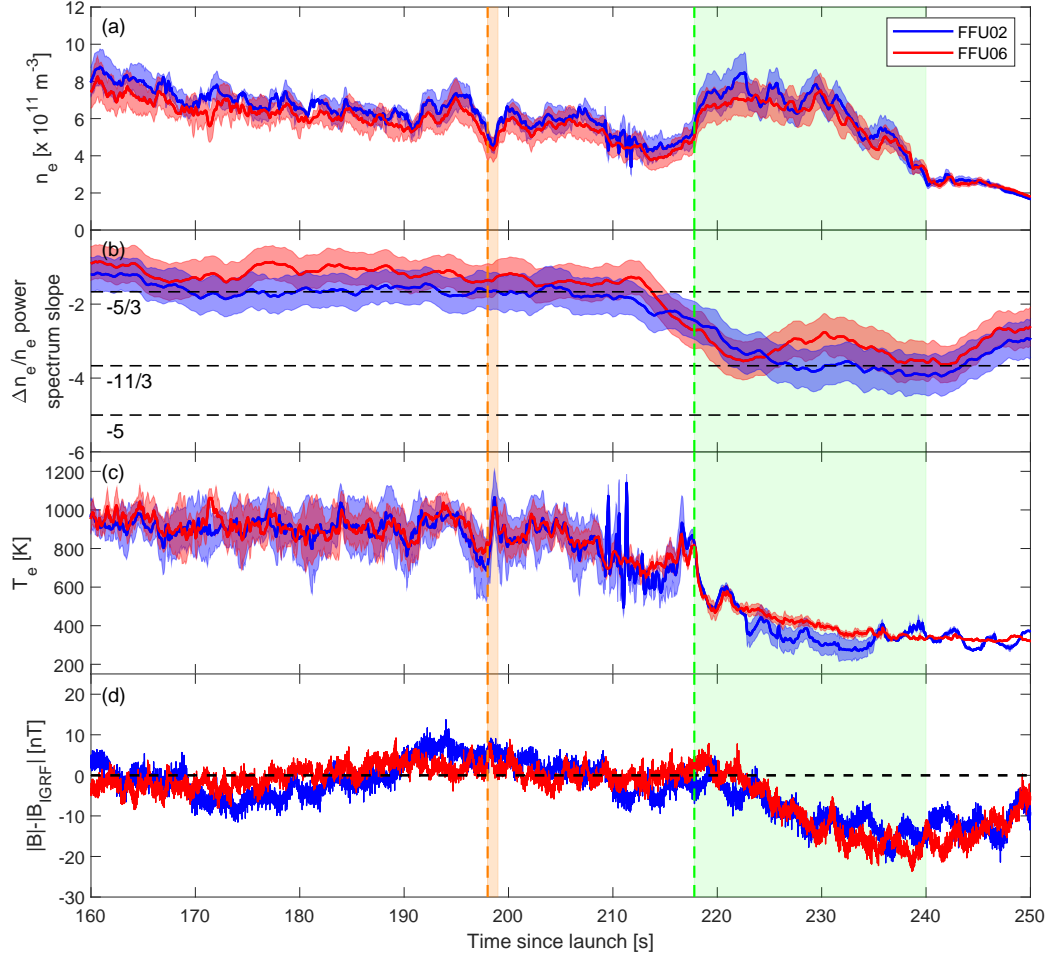


Figure 6. Time series for the electron density (a), the slope of the detrended relative density power spectrum (b), the electron temperature (c) and the total magnetic field residual (d), for FFU02 (blue) and FFU06 (red). The vertical orange dash line at 198 s shows the first event, with a decrease in density and temperature followed by a sharp increased in temperature with delayed increase in density (shown by the orange shaded column). The vertical green dash line at 218 s indicates the start of the second event, *i.e.* the density enhancement region, shown by the green shaded column until 240 s.

6 Conclusion

The SPIDER sounding rocket presented the first *in situ* multi-point measurements of the plasma properties and electric field inside an auroral electrojet. Although only six of the ten ejected free falling units were recovered, and beside some issues during the flight (*i.e.* unexpectedly large payload charging saturating the recorded current and wobble-induced short-circuits), usable Langmuir probe measurements were obtained on two different FFUs. Due to an intermediate plasma regime where the thickness of the plasma sheath was comparable to the probe radius, the full analytical formulation of ion collecting by a moving spherical body was used to interpret the measured current. An empirical estimation of the sheath thickness was required to perform the fitting of the I - V curves. Empirically, values between 10 and 20 mm were used (depending on the probe potential with respect to plasma). Indirect confirmation of this assumption was obtained by modelling the FFU and Langmuir probe using the SPIS software, providing good match to the I - V curve measurements and the sheath thickness used for the fitting and thus bolstering the confidence in the analytical results.

In addition, a direct confirmation of the plasma parameters retrieved by the FFUs was provided by incoherent scatter radar measurements along the rocket path from the EISCAT facility in Tromsø. Both measurements were not exactly taken at the same time, with EISCAT sampling the up-leg while the useful Langmuir probe measurements from the FFUs were taken mostly during the down-leg. Yet, the magnitude and structure of the electron density and temperature as a function of altitude is comparable: both detected a denser ($6 \times 10^{11} \text{ m}^{-3}$) and hotter (1000 K) electron population above 120 km compared to a less dense ($1\text{--}2 \times 10^{11} \text{ m}^{-3}$) and cooler (400 K) below.

Thus, with confidence in the FFU measurements, two events were discussed in more details. First, a sharp decrease in both electron density and temperature was seen around 198 s after launch. This event happened on a 1-2 km spatial scale, and is therefore likely to be of temporal nature, e.g. local precipitation along a field line. The second event occurred at 218 s after launch, where a significant increase in electron density can be seen for more than 20-30 s. The increased density is accompanied by a large decrease in the electron temperature. A tomography-like reconstruction of the auroral volume emission rate based on the ground-based observation from the ALIS system confirmed that this increase in electron density was due to the FFUs entering an horizontal layer between 120 and 130 km with larger emission rate. ALIS also revealed a temporal increase of the volume emission rate in this layer around the same time, thus indicating larger electron precipitation. The measured magnetic field inside the layer was seen to be ~ 15 nT less than the expected magnetic field from the IGRF model, indicating a Hall current is produced by the increased electron precipitation in the layer. In addition, the power spectrum of the electron density variations was studied to look for hints of turbulence, and a different slope of $-11/3$ compared to the typical Kolmogorov regime of $-5/3$ was observed. Such power spectrum slope could be an indication of drift wave instabilities, possibly induced by the increased electron precipitation.

In conclusion, this article demonstrated the need for instruments with high spatial and temporal resolutions to investigate auroral multi-scale processes. In this respect, sounding rocket are the ideal platform to carry such instruments. This work also pointed out the important of utilising ground-based facilities (ALIS and EISCAT) to provide context observations to the rocket-borne measurements.

A Retrieval of the plasma parameters: ion accelerated current and sheath thickness assumption.

This section presents the details of the plasma parameters retrieval, in particular the expression of the ion accelerated current I_{acc} and the assumption taken regarding the sheath thickness around the probe.

Assuming no collisions take place inside the sheath and the particle distribution outside the sheath is Maxwellian with a superimposed drift velocity, the general formulation of I_{acc} for a moving spherical probe was given by Warthon and Hoegy [1971]

$$\begin{aligned}
 I_{\text{acc}} = & \left(\frac{a}{r}\right)^2 \left[\frac{\sqrt{\pi}}{2} \frac{(M^2 + \frac{1}{2})}{M} \text{erf}(M) \right. \\
 & + \frac{\sqrt{\pi}}{2} \frac{W}{2M} [\text{erf}(M - \gamma W^{1/2}) + \text{erf}(M + \gamma W^{1/2})] + \frac{1}{2} e^{-M^2} \Big] \\
 & - \left(\left(\frac{a}{r}\right)^2 - 1 \right) \left[\frac{\sqrt{\pi}}{2} \frac{(M^2 + \frac{1}{2} + W)}{2M} [\text{erf}(M - \gamma W^{1/2}) + \text{erf}(M + \gamma W^{1/2})] \right. \\
 & \left. + \frac{M + \gamma W^{1/2}}{4M} e^{-(M - \gamma W^{1/2})^2} + \frac{M - \gamma W^{1/2}}{4M} e^{-(M + \gamma W^{1/2})^2} \right]
 \end{aligned} \tag{A.1}$$

in which the variables W , M , γ and a are defined as

$$W = \frac{e | (V - V_p) |}{k_B T_i}, \quad M = \frac{m_i v^2}{2k_B T_i}, \quad \gamma = \frac{1}{\sqrt{(a/r)^2 - 1}}, \quad a = r + h$$

where h is the sheath thickness, v is the velocity of the probe inside the plasma, and m_i the mass of the ions. Here, v was obtained from FFU GPS recordings, and m_i is taken as 31 atomic unit which is the average mass of the two most common species of ions at this altitude: O_2^+ and NO^+ . Note that this expression greatly simplified in the thin-sheath region ($a/r \rightarrow 1$) or the large-sheath region ($a/r \gg 1$) and respectively reduces to similar expression as presented by *Sagalyan et al.* [1963] and *Fahleson et al.* [1974]. It is important to notice that Equation (A.1) is expressed as a function of the ion temperature T_i . However, the Bohm criterion [Riemann, 1991] implies that, in order for the sheath to be stable, only ions with a velocity large enough to overcome the electrostatic potential of the sheath are able to reach the probe. This threshold velocity corresponds to a equivalent ion thermal motion induced by a temperature of at least $T_e/2$. Hence, one interpretation is that ions are accelerated towards the probe by the pre-sheath potential. Collectively, the collected ions can be seen to have a temperature equal or larger than $T_e/2$. This temperature is higher than for the undisturbed ions far from the probe, thus making the true ion temperature impossible to evaluate in this intermediate sheath regime. Following this assumption, every instances of T_i in the expression of W and M was replaced by $T_e/2$ instead, making the ion current a function of the electron temperature.

An estimation of the sheath thickness h is required in order to use Equation (A.1). The general sheath equation was given by *Chen* [1979] in a one-dimensional case as

$$\frac{1}{2} \left(\frac{d\eta}{d\xi} \right)^2 = \mathfrak{M}^2 \left[\sqrt{\left(1 + \frac{2\eta}{\mathfrak{M}^2} \right)} - 1 \right] + e^{-\eta} - 1 \quad (\text{A.2})$$

where the variables ξ , η and \mathfrak{M} are

$$\xi = \frac{h}{\lambda_{Ds}}, \quad \lambda_{Ds} = \sqrt{\frac{\varepsilon_0 k_B T_e}{e^2 n_s}}, \quad \eta = \frac{e|V - V_p|}{k_B T_e}, \quad \mathfrak{M} = \sqrt{\frac{m_i v_i^2}{k_B T_e}}.$$

In these variables, λ_{Ds} is the Debye length estimated at the sheath edge where $n_s = e^{-1/2} \times n_e$, ε_0 is the vacuum permittivity and v_i is the velocity of the ions. An important simplification is taken here: Equation A.2 was derived for a one-dimensional case but is here applied to a three-dimensional case. The spherical symmetry of the SPIDER probes is used to assume the three-dimensional case to be equal to a one-dimensional case along the radial direction.

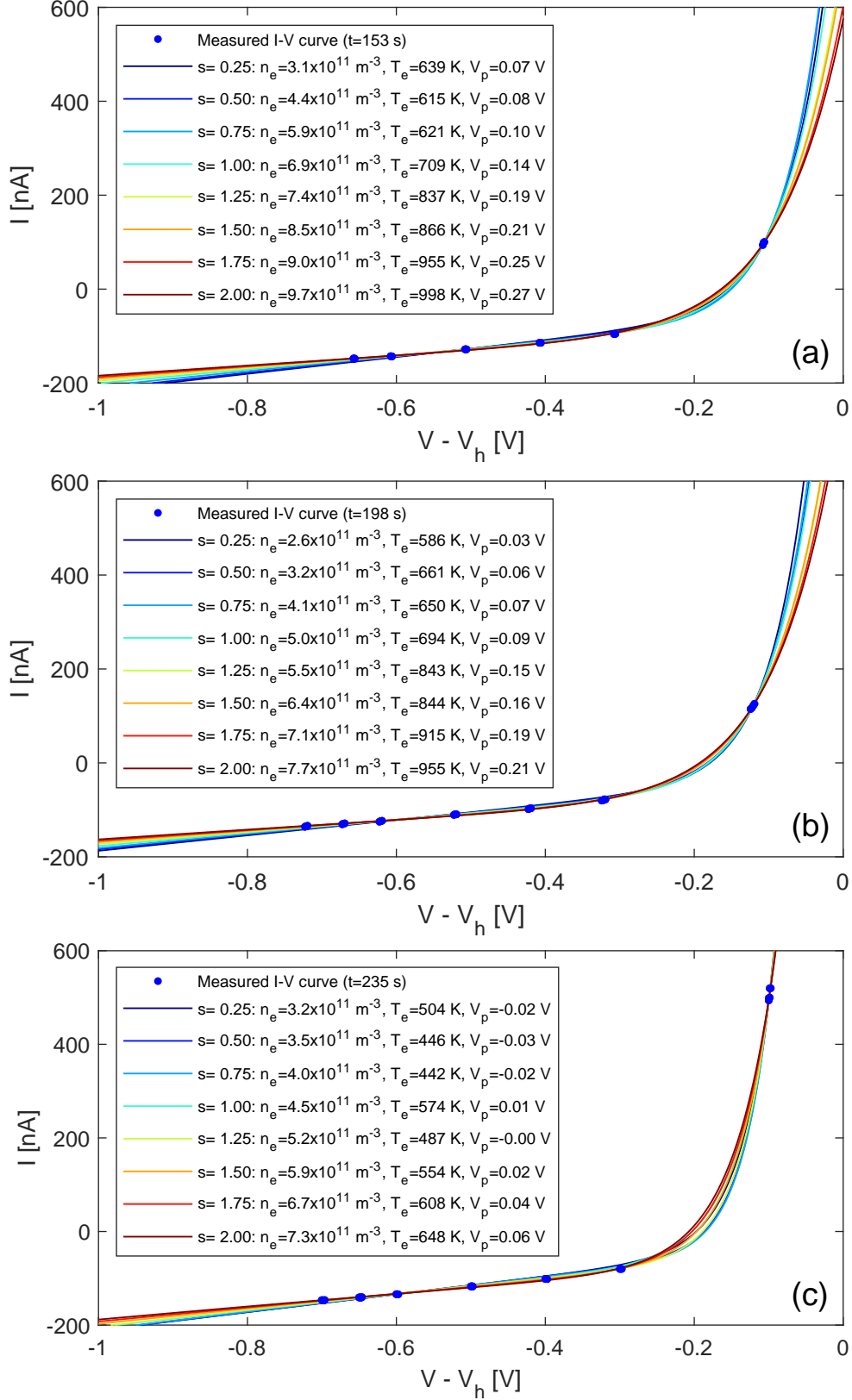
A relationship between η and ξ can be obtained by numerically integrating the following differential equation

$$d\eta/d\xi = \sqrt{2} \left[\sqrt{1 + 2\eta} + e^{-\eta} - 2 \right]^{1/2} + s \quad (\text{A.3})$$

where s corresponds to the slope of the electrostatic potential at the edge of the sheath. One can notice that this expression tends towards the Child-Langmuir law for large value of ($\eta > 100$) but diverges depending on the value of s for smaller η where the Child-Langmuir law is not valid any more. Here, η is expected to be between 1 and 20, for the two extreme cases where the probe potential and electron temperature are 0.1 V and 1000 K, and 0.7 V and 400 K, respectively. Hence, the parameter s cannot be neglected in the presented case. Estimating this parameter solely based on the I - V curve is impossible since such measurement does not contain any direct information about the shape of the potential around the probe. However, leaving it as a free parameter to be fitted along side with the other plasma parameters leads to unrealistic results, as it competes with T_e . Although s is not necessarily constant along the trajectory, as the shape of the potential around the probe could be influenced by the plasma environment, one can assume that the influence of the external magnetic field and of the probe properties (*e.g.* capacitance, surface roughness, etc.) are the main factors affecting the shape of the potential. In this case, the assumption of a constant s can be taken. Note that a constant s does not imply a constant sheath thickness, as the plasma density, temperature, and the probe bias potential, are present in Equation (A.3).

Figure A.1 shows three examples of measured I - V curves taken at different times during the flight. The potential of the probe is expressed with respect to the hull potential after correction of two effects: the charging of the hull (~ -0.8 V) and the ambient electric field (up to ± 0.03 V depending

on the orientation of the probe). The influence of changing the probe bias steps on the hull charging was negligible (~ 10 mV) and not included in the correction. Fittings using constant s values from 0.25 to 2 are shown in Figure A.1. One can see that values of s below 1 do not match the trend seen in the ion saturation. Overall, larger values of s provide a better fit to the measured I - V curves, while reporting higher electron density, electron temperature and plasma potential. However, larger values of s imply a sharper potential drop at the sheath edge which is physically unlikely. Thus, the smallest values of s which gives a reasonable fit to the measured ion saturation current should be used.



332 **Figure A.1.** Example of I - V curves measured by FFU06 at (a) 153 s, (b) 198 s and (c) 235 s. Blue dots
 333 shows the measured current, while solid lines from blue to red shows the fitting for s from 0.25 to 2.00.

In the case of SPIDER, a s value between 1 and 1.5 provided a satisfying fit for the I - V curves along the entire flight while keeping s relatively small. The mean value obtained from fitting Equation (1) with s equal to 1 and 1.5 was considered for the mean plasma parameters, while the difference gauged the uncertainty of the method on each of the plasma parameters.

B Confirmation with SPIS simulation

Results from Appendix A are based on an empirical value of s which dictates the shape of the electrostatic potential around the probe. This leads to a sheath thickness between 6 to 18 mm for the probe bias between +0.7 V and +0.1 V, respectively (when considering a charging of the hull to -0.8 V and a plasma potential around -0.35 V). Hybrid plasma simulations using the Spacecraft Plasma Interaction Software [SPIS, Roussel *et al.*, 2008] were used to confirm the assumption taken. A model of the FFU with one of its spherical Langmuir probe was simulated inside a plasma of similar density and temperature as derived in Section 3, *i.e.* n_e equals to $5 \times 10^{11} \text{ m}^{-3}$ and T_e equals to 900 K. The FFU was given an horizontal velocity of 500 m/s, similar to the velocity around the apogee, while the plasma was kept stationary in the simulated volume, thus including the ion ram-current. Figure B.1 shows the geometry of the configuration by displaying the shape of the electrostatic potential in two perpendicular planes. A rougher mesh was used around the FFU compared to the finer mesh around the probe, as the main interest was to investigate the plasma sheath around the latter.

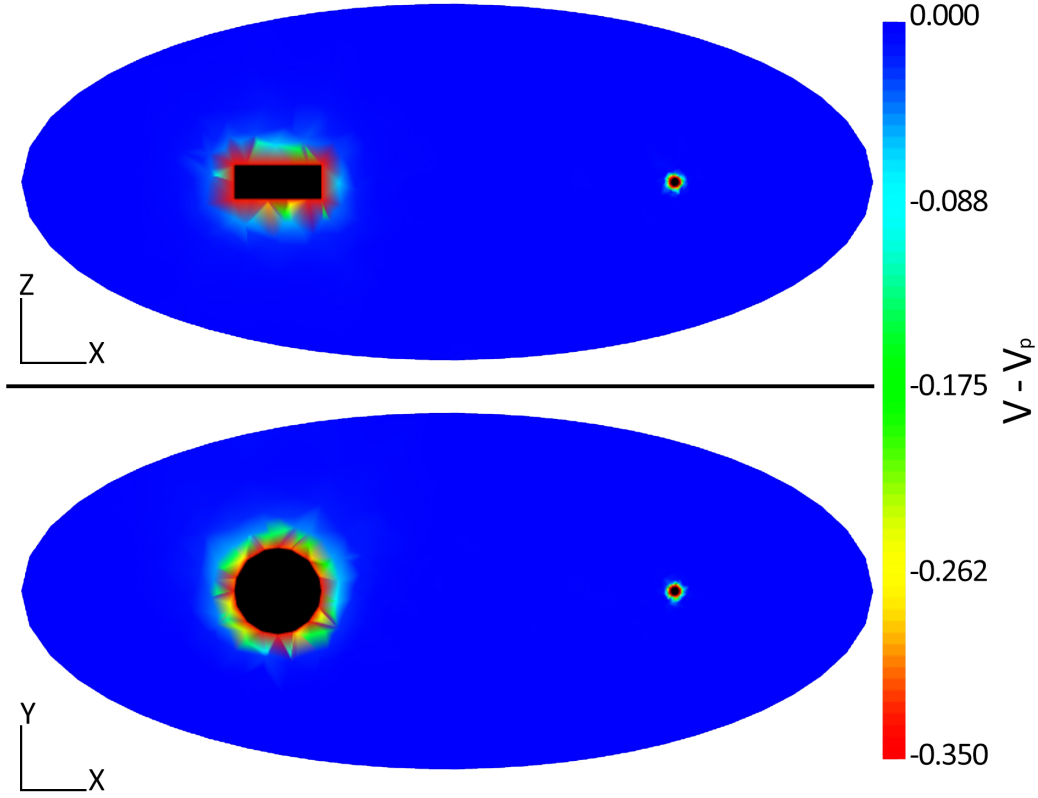


Figure B.1. XZ (top) and XY (bottom) cut of the simulated plasma potential around the disc-shape FFU (on the left) and the spherical Langmuir probe (on the right, 1 m away).

The simulation provided the current collected by each surface, as well as the spatial distribution of the potential, electron density and ion density around the probe. Several runs were performed for

biases of the probe ranging from -0.5 to $+0.2$ V with respect to the FFU body. The simulated payload charging was around -0.35 V with respect to plasma potential, which is only about half the one observed in flight by the electric field probes. Nonetheless, both the simulated floating potential with respect to plasma potential and collected current by the probe were very similar to the measured one, as is shown in Figure B.2(a). The error bars are the $2\text{-}\sigma$ error calculated based on the fluctuation of the collected current during the part of each simulation run after which the equilibrium state if the plasma was achieved. Errors mostly come from ions due to the particle-in-cell approach taken to simulate their motion, thus increasing the fluctuation of the collected current between each timestep. In addition, the sheath thickness was obtained for each of these cases, determined as the distance from the probe where the electron density (averaged radially around the probe) drops below 60% of its undisturbed value ($e^{-1/2} \times n_e$, as defined by *Chen* [1979]). The simulated sheath thickness was compared to the values used during the analytical fitting with s equal to 1 and 1.5, as presented in Figure B.2(b). Again, a good agreement is seen between the simulation and the analytical method, especially for larger potential difference. This can be explained as the simulation struggles to properly define the sheath when the probe potential approaches the plasma potential, where the sheath collapses (*i.e.* start of the electron saturation). Error bars are the corresponding $2\text{-}\sigma$ error derived from the $2\text{-}\sigma$ error on the average radial electron density, itself calculated as the standard deviation of the electron density profiles in all radial directions.

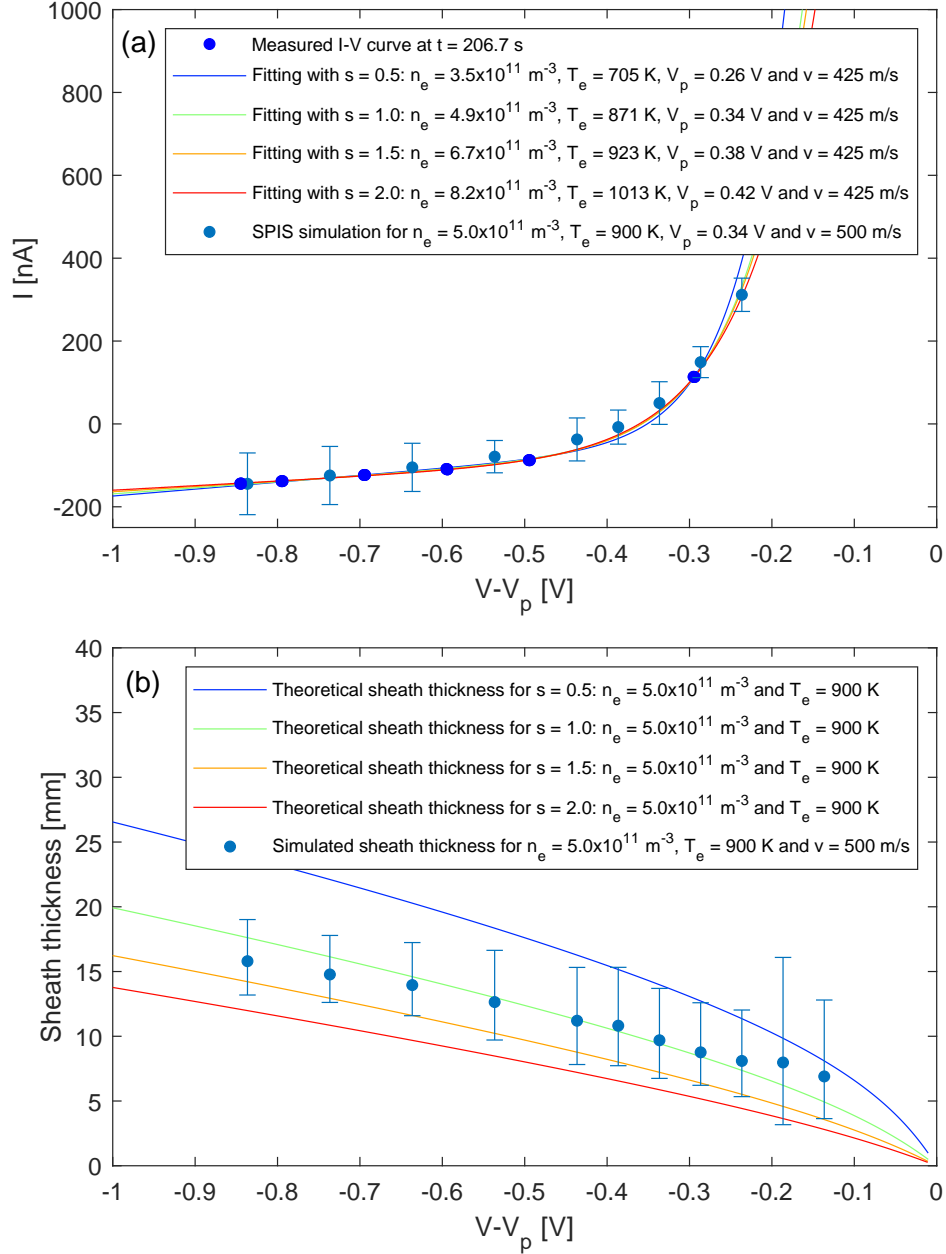


Figure B.2. (a) Comparison between measured, fitted and simulated I - V curves. Blue dots shows a measured I - V curve from FFU06. The blue, green, orange and red solid lines shows the fitting with s equal to 0.5, 1, 1.5 and 2.0, respectively. Grey dots show the simulated I - V curve from SPIS, with $\pm 2\text{-}\sigma$ error bars. (b) Comparison between the sheath thickness assumed for the analytical retrieval of the plasma parameters and the simulated sheath thickness for similar plasma parameters using SPIS. The blue, green, orange and red solid lines show the fitting with s equal to 0.5, 1, 1.5 and 2.0, respectively. Grey dots show the simulated sheath thickness with $\pm 2\text{-}\sigma$ error bars.

Moreover, the simulated potential around the probe was used to estimate the value of s . Figure B.3(a) shows the radial electron distribution around the probe (mean and $\pm 2\text{-}\sigma$ limits) for a probe bias of -0.4 V with respect to the hull. Based on the criteria from *Chen* [1979] the sheath thickness was estimated between 12.6 and 17.8 mm. The shape of the potential around the probe (mean and

385 $\pm 2\text{-}\sigma$ limits) is shown in Figure B.3(b). s is calculated as the first derivative of the normalized po-
 386 tential (*i.e.* $d\eta/d\xi$) and estimated for the minimum, mean and maximum cases of both the sheath
 387 thickness and the potential as 0.06, 0.33 and 0.91, respectively. The slope of the simulated potential
 388 at the sheath edge is not as sharp as expected from the analytical expression, with values of s likely
 389 closer to 0.5. Nevertheless, a s value around unity is still within the simulation uncertainty.

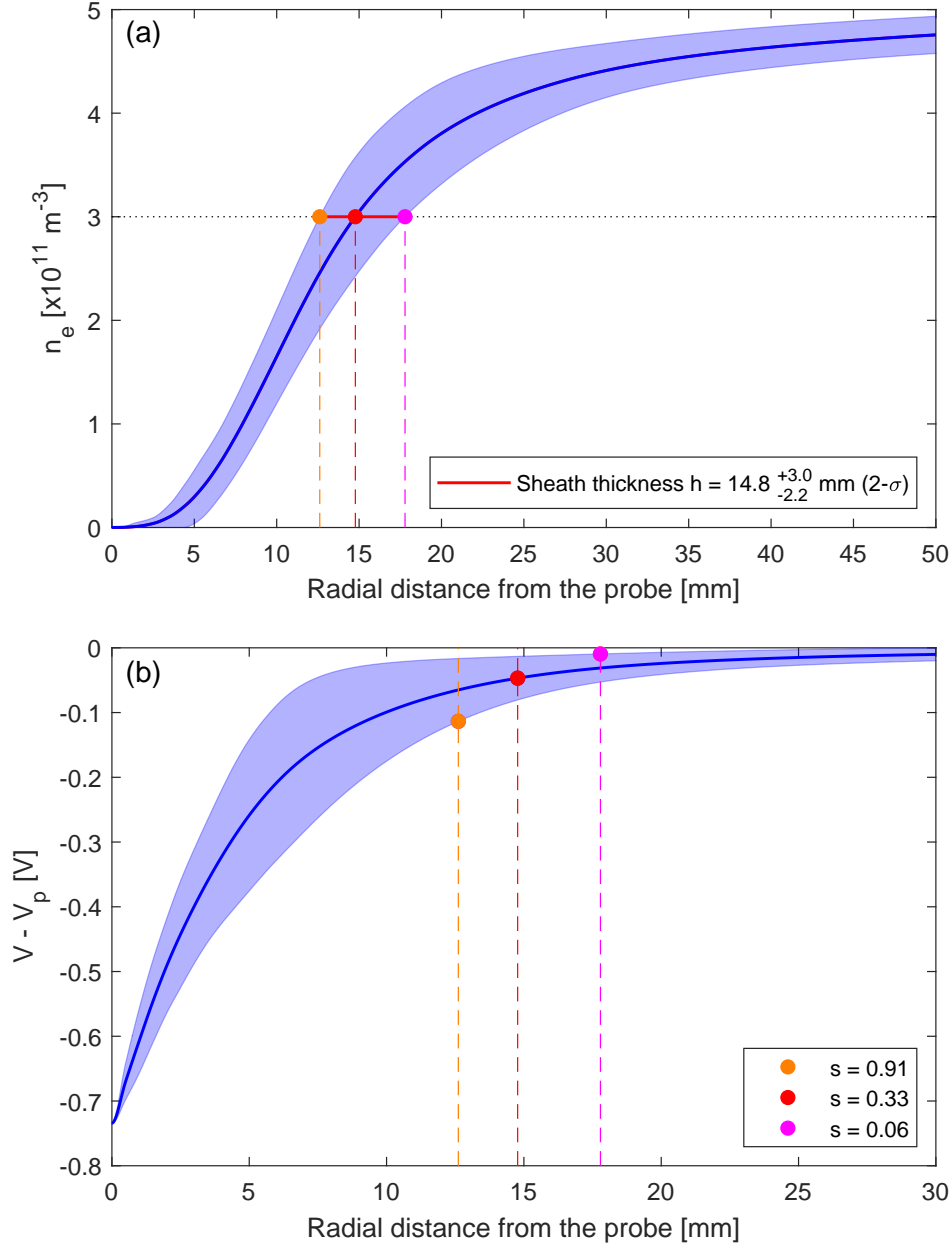


Figure B.3. (a) Simulated radial electron density distribution around the probe for a probe bias of -0.4 V with respect to the hull. The blue shaded area shows the $\pm 2\sigma$ uncertainty. The threshold for the sheath thickness is $3 \times 10^{11} \text{ m}^{-3}$ (i.e. $\sim e^{-1/2} \times n_e$), leading to a sheath thickness between 12.6 and 17.8 mm. (b) Simulated radial potential profile around the probe for a probe bias of -0.4 V with respect to the hull. The blue shaded area shows the $\pm 2\sigma$ uncertainty. The orange, red and magenta dots show the value of s (i.e. derivative of the potential at the sheath edge) for the upper, mean and lower cases corresponding to the sheath thickness uncertainty from (a).

Although the SPIS simulation did not reproduce the exact payload charging observed during flight, it provides compelling evidence to support the analytical method used to interpret the flight measurements, both in term of the collected current by the probe and of the sheath thickness around it. The simulated potential at the sheath edge is not as sharp as the values used analytically, with s

values between 0.1 and 1.0 compared to 1.0 and 1.5. This might be due to a discrepancy between the 1-D analytical expression and the 3-D simulation. On the other hand, the simulated sheath thickness still matches the analytical cases with s between 1.0 and 1.5. However, this confirms that a sharp potential at the sheath edge is unphysical, and therefore large values of s should not be considered.

Acknowledgments

The work was partially supported by the Swedish Government Agency for Innovation Systems (VINNOVA) contract no. 2016-04094. The SPIDER sounding rocket project was supported by the Swedish National Space Agency. The data from the SPIDER sounding rocket used in this article is hosted by the Swedish National Data Service under SND-ID: 2021-38.

References

- Oppenheim, M. M. and Dimant, Y. S. (2013). Kinetic simulations of 3-D Farley-Buneman turbulence and anomalous electron heating. *J. Geophysical Research: Space Physics*, 118, doi:10.1002/jgra.50196
- Warthon, L. E. and Hoegy, W. R. (1971). Current to moving spherical and cylindrical electrostatic probes. *NASA Goddard Space Flight Center internal report*, X-621-71-276
- Sagalyn, R. C., Smiddy, M. and Wisnia, J. (1963). Measurement and interpretation of ion density distribution in the daytime F region. *J. Geophysical Research*, 68
- Fahleson, U., Falthammar, C. G. and Pedersen, A. (1974). Ionospheric temperature and density measurements by means of spherical double probes. *Planet. Space Sci.*, 22
- Pedersen, A. et al. (2008). Electron density estimations derived from spacecraft potential measurements on Cluster in tenuous plasma regions. *J. Geophysical Research*, 113, doi:10.1029/2007JA012636
- Roussel, J.-F. et al. (2008). SPIS Open Source Code: Methods, Capabilities, Achievements and Prospects. *IEEE Transactions on Plasma Science*, 36, 2360-2368, doi:10.1109/TPS.2008.2002327
- Chen, F. (1979). Thickness of combined Bohm-Langmuir sheaths. *Unclassified TRW report*, Task II-2186, url:<http://www.seas.ucla.edu/ffchen/Archive/Chen087.pdf>
- Mott-Smith, H. M. and Langmuir, I. (1926). The theory of collectors in gaseous discharges. *Physical Review*, 28, 727-763
- Riemann, K. U. (1991). The Bohm criterion and sheath formation. *J. Phys. D: Appl. Phys*, 24, 493, doi:10.1088/0022-3727/24/4/001
- Barjatya, A. and Swenson, C. M. (2006). Observations of triboelectric charging effects on Langmuir-type probes in dusty plasma. *J. Phys. D: Appl. Phys*, 111, A10302, doi:10.1029/2006JA011806
- Brändström, U. (2003). The Auroral Large Imaging System - Design, Operation and Scientific Results. *PhD thesis*, IRF Scientific Report 279, ISBN 91-7305-405-4, Kiruna
- Kintner, P. M. and Seyler, C. E. (1985). The status of observations and theory of high latitude ionospheric and magnetospheric plasma turbulence. *Space Science Reviews*, 41, 91-129, doi:10.1007/BF00241347
- Spicher, A., Miloch, W. J. and Moen, J. I. (2014). Direct evidence of double-slope power spectra in the high-latitude ionospheric plasma. *Geophys. Res. Lett.*, 41, 1406-1412, doi:10.1002/2014GL059214
- Macmillan, S., Maus, S., Bondar, T. et al. (2003). Ninth Generation International Geomagnetic Reference Field Released. *AGU*, 81, 46, 503-503, url:<https://ccmc.gsfc.nasa.gov/models/modelinfo.php?model=IGRF>